Int J Adv Manuf Technol (2002) 20:169–179

The International Journal of
Advanced
Manufacturing
Technology

Design and NC Machining of Concave-Arc Ball-End Milling Cutters

W.-F. Chen, H.-Y. Lai, and C.-K. Chen

Department of Mechanical Engineering, National Cheng-Kung University, Tainan, Taiwan

The paper presents a geometric modelling approach for the precision design and NC machining of a concave-arc ball-end milling (CABEM) cutter which is an important tool for mould-making industries. This paper presents systematic models of the cutting edge, helical groove, and grinding wheel design for the NC machining of a CABEM cutter. Both the normal to the revolving axis and the tangent to the groove, are used to derive the required precision sectional profiles of the grinding wheel. In compliance with the maximal sectional radius of the cutter, the profile of the groove section and both the radial and axial cutting speeds of the grinding wheel are computed in sequence. Using the computer simulation results of the groove actually obtained, this paper proposes a method to resolve the problems of the residual revolving surface and the narrow cutting edge strip. This paper is intended to serve as a reference for the design and NC machining of cutters of this type.

Keywords: Concave-arc ball-end milling cutter; Helical groove; NC machining; Reverse engineering

1. Introduction

The increase in product machining has led to ever increasing demands being placed upon the revolving cutters employed in the NC machining of freeform and complex surfaces of dies and moulds. These revolving cutters feature helical cutting edges and grooves to facilitate both milling and chip removal. The precise shape of the cutter is not fixed; it varies according to the particular machining situation for which it is being used. For this reason, studies relating to revolving cutters are both broad in scope and versatile in application.

There have been many studies relating to the design of this type of revolving cutter [1–5]. The manufacturing theory of this cutter type is discussed in [6,7], and the specific problems relating to the manufacture of this type of cutter using a forming cutter are discussed in [8–10]. Monitoring during the machining process has been investigated [11–14], and the cutting edge and its smooth conjunction has been studied [15, 16]. Zhou et al. [17,18] studied the forming principle and the position of the rake plane. Finally, issues relating to the normal section of the helical groove, the manufacturing process, cutting parameters and cutter measurement have been discussed [19–21]. Although it is difficult to identify the exact number precisely, there are only a few papers which discuss both the design of the cutting edge and the NC machining of the helical groove.

As mentioned in [22], revolving cutters have different shapes, including cylinder-shaped, cone-shaped, concave-arc shaped, torch-shaped, and involute-shaped. Although revolving cutters with concave-arcs have been widely used, it is not easy to locate papers which deal with this cutter type. They are mentioned by Tang and Chen [23], but little detail is provided. For this reason, this paper will focus upon issues relating to this type of cutter.

A review of work carried out on this type of cutter reveals that most studies concern themselves only with the design of the helical cutting edge and the groove section [24–26]. Other papers discuss the NC machining of the rake face or of the helical groove by multiple machining processes. One problem is that most studies have been too far removed from actual engineering applications, or require complicated manufacturing processes, which are expensive to implement in the real machining world.

To redress this problem, this paper will present not only the design models for the cutting edge and helical groove, but also models of section design, feed speeds and the relative displacement of the grinding wheel during NC machining of the cutter. The models of actually obtained cutting edges and grooves will also be presented, together with a proposed method to rectify the problems of the residual revolving surface and narrow cutting strip.

It will be shown that a reverse engineering process for the envelope is essential. The enveloping surface, i.e. the groove surface should be designed first, followed by the definition of the profile and relative motion of the grinding wheel.

Correspondence and offprint requests to: W.-F. Chen, Department of Mechanical Engineering, National Cheng-Kung University, Tainan, Taiwan 701. E-mail: wfchen1@ms35.hinet.net

2. Profile Design of the Ball-End Cutter with Concave-Arc Generator

As shown in Fig. 1, the profile of a revolving cutter with a concave-arc generator is formed by rotating the curve *ABCD* around the *z*-axis. The radius of arc *AB* is *R*. The centre angle of arc *BC* should be determined by the particular engineering situation. The centre-point *Q* of arc *BC* may have many different positions relative to the centre-point *P* of arc *AB*. Only the case where the straight line *PQ* is perpendicular to the *z*-axis is dealt with in this paper. The radius of concave arc *BC* is R_1. *CD* is a straight line parallel to the *z*-axis. The revolving surfaces formed by *ABCD* can be expressed by a sectional-continuous function.

The equation of the revolving surface corresponding to arc *AB* can be expressed as follows:

$$\boldsymbol{r}_1 = \{\sqrt{(R^2 - z^2)}\cos\phi,\ \sqrt{(R^2 - z^2)}\sin\phi,\ z\}, \quad z \in [-R, 0], \quad \phi \in [0, 2\pi] \tag{1}$$

The equation of the revolving surface corresponding to arc *BC* can be expressed as follows:

$$\boldsymbol{r}_2 = \{(R + R_1 - R_1\cos\theta_1)\cos\phi,\ (R + R_1 - R_1\cos\theta_1)\sin\phi,\ R_1\sin\theta_1\}, \quad \theta_1 \in [0, \alpha], \quad \phi \in [0, 2\pi] \tag{2}$$

The equation of the revolving surface corresponding to line *CD* can be expressed as follows:

$$\boldsymbol{r}_3 = \{(R + R_1 - R_1\cos\alpha)\cos\phi,\ (R + R_1 - R_1\cos\alpha)\sin\phi,\ R_1\sin\alpha + h\}, \quad \phi \in [0, 2\pi], \quad h \in [0, h_1] \tag{3}$$

3. Cutting Edge on the Revolving Surface

The cutting edge on the revolving surface formed by arc *AB* is a helical curve which has a constant angle ψ with the generator curve.

From Eq. (1), it is known that:

$$\begin{cases} \boldsymbol{r}_{1\theta} = \left\{-\dfrac{z}{\sqrt{(R^2 - z^2)}}\cos\phi,\ -\dfrac{z}{\sqrt{(R^2 - z^2)}}\sin\phi,\ 1\right\} \\ \boldsymbol{r}_{1\phi} = \{-\sqrt{(R^2 - z^2)}\sin\phi,\ \sqrt{(R^2 - z^2)}\cos\phi,\ 0\} \end{cases} \tag{4}$$

$$\begin{cases} E = \boldsymbol{r}_{1z}{}^2 = \dfrac{z^2}{R^2 - z^2} \\ F = \boldsymbol{r}_{1z} \bullet \boldsymbol{r}_{1\phi} = 0 \\ G = \boldsymbol{r}_{1\phi}^2 = R^2 - z^2 \end{cases} \tag{5}$$

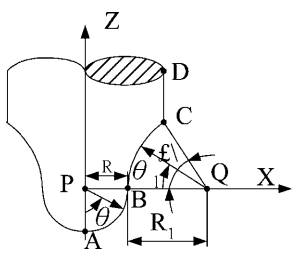

Fig. 1. Concave-arc ball-end milling cutter.

Let the tangent vector of the point on the cutting edge be d$\boldsymbol{r}$ and the tangent vector of the point on the generator curve be $\delta\boldsymbol{r}$. It will be seen that:

$$\begin{cases} \mathrm{d}\boldsymbol{r} = \boldsymbol{r}_{1z}\mathrm{d} + \boldsymbol{r}_{1\phi}\mathrm{d}\phi \\ \delta\boldsymbol{r} = \boldsymbol{r}_{1z}\delta z \end{cases} \tag{6}$$

According to the definition of the dot product of two vectors, it is known that the angle ψ between d$\boldsymbol{r}$ and $\delta\boldsymbol{r}$ is determined as follows:

$$\cos^2\psi = \frac{(\mathrm{d}\boldsymbol{r}_1 \bullet \delta\boldsymbol{r}_1)^2}{|\mathrm{d}\boldsymbol{r}_1|^2\,|\delta\boldsymbol{r}_1|^2} = \frac{E\mathrm{d}z^2}{E\mathrm{d}z^2 + G\mathrm{d}\phi^2} \tag{7}$$

i.e.

$$\mathrm{d}\phi = \tan\psi\sqrt{\left(\frac{E}{G}\right)}\,\mathrm{d}z = \frac{R}{R^2 - z^2}\,\mathrm{d}z \tag{8}$$

After integration, Eq. (8) becomes:

$$\phi_1 = R\tan\psi\int_0^z \frac{1}{R^2 - z^2}\,\mathrm{d}z = \tfrac{1}{2}\tan\psi\ln\frac{R + z}{R - z} \tag{9}$$

The cutting edge may be obtained by substituting Eq. (9) into Eq. (1). For the revolving surface formed by arc *BC*, we have:

$$\begin{cases} \mathbf{r}_{2\theta_1} = \{R_1\sin\theta_1\cos\phi,\ R_1\sin\theta_1\sin\phi,\ R_1\cos\theta_1\} \\ \mathbf{r}_{2\phi} = \{-(R + R_1 - R_1\cos\theta_1)\sin\phi,\ (R + R_1 - R_1\cos\theta_1)\cos\phi, 0\} \end{cases} \tag{10}$$

$$\begin{cases} E = \mathbf{r}_{2\theta_1}^2 = R_1^2 \\ F = \mathbf{r}_{2\theta_1} \bullet \mathbf{r}_{2\phi} = 0 \\ G = \mathbf{r}_{2\phi}{}^2 = (R + R_1 - R_1\cos\theta_1)^2 \end{cases} \tag{11}$$

Accordingly, we can obtain:

$$\mathrm{d}\phi = \tan\psi\sqrt{\left(\frac{E}{G}\,\mathrm{d}\theta_1 = \frac{R_1\tan\psi}{R + R_1 - R_1\cos\theta_1}\,\mathrm{d}\theta_1\right.} \tag{12}$$

After integration, Eq. (12) becomes:

$$\phi_2 = \frac{2R_1}{R + R_1}\tan\psi\ \mathrm{cosec}\ \alpha^*\tan^{-1}\left(-\mathrm{cosec}\ \alpha^*\tan\frac{\pi/2 - \theta_1}{2} + \cot\alpha^*\right) + C \tag{13}$$

where:

$$\alpha^* = \cos^{-1}\frac{R_1}{R + R_1}$$

In accordance with the initial condition that $\phi_2 = 0$ when $\theta_1 = 0$, we find:

$$C = -\frac{2R_1}{R + R_1}\tan\psi\ \mathrm{cosec}\ \alpha^*\tan^{-1}(\cot\alpha^* - \mathrm{csc}\alpha^*) \tag{14}$$

Substituting the constant *C* into Eq. (13), given:

$$\phi_2 = \frac{2R_1}{R + R_1}\tan\psi\ \mathrm{cosec}\ \alpha^*\tan^{-1}\left(-\mathrm{cosec}\ \alpha^*\tan\frac{\pi/2 - \theta_1}{2} + \cot\alpha^*\right) - \frac{2R_1}{R + R_1}\tan\psi\ \mathrm{cosec}\ \alpha^*\tan^{-1}(\cot\alpha^* - \mathrm{csc}\alpha^*) \tag{15}$$

4. Design of the Helical Grooves on the Ball-End

Since the radius of the cross-section of the revolving cutter is variable in the z-direction, the section of the groove also varies; its depth decreases in the direction of the increasing z-coordinate. During NC machining of the cutter it is not possible to change the section profile of the grinding wheel according to variations in cutter radius. To overcome this problem, the section design of the cutter groove may be defined based on the maximum radius of the cutter. A process of reverse engineering of the profile envelope which fits the required groove section may be used to determine the required section of the grinding wheel. Adjusting the feed of the grinding wheel in the radial direction controls the depth of the groove. It is necessary to check the groove actually obtained and then to carry out a rectification operation so as to ensure that the correct profile is obtained. We now consider issues relating to the groove.

On the x,y-plane, the model of the groove section can be defined by the equation of the curves and the coordinates of the connecting points. The equation of the straight line GH may be defined as:

$$\mathbf{r}_{GH} = \{R_2,0\} + \xi_0\{\cos\delta, -\mathrm{din}\delta\} \tag{16}$$

where R_2 is the outer radius of the cross-section and ξ_0 is the length parameter used for describing an arbitrary point on segment GH. The centre of arc HI is the point E and the radius is given as r_1. The centre of the inner land circle is the point O and the radius is given as r_b. In other words, the distance OE is given by $r_b + r_1$, and point E can be located at the intersection point of a circle centred at point O with a radius $r_b + r_1$, and a line parallel to line GH at a distance r_1. Thus, $G(R_2,0)$, $L(-R_2 \sin(\pi/6), R_2 \cos(\pi/6)$ and the position vector of point E and the parallel line $G'H'$ can be mathe matically expressed as

$$\begin{aligned}\mathbf{r}_E &= \{x_E,y_E\} = \{R_2 + \xi_0 \cos\delta - r_1 \sin\delta, -\xi_0 \sin\delta + r_1 \cos\delta\} \\ &= \{(r_1 + r_b)\cos\eta_1, (r + r_b)\sin\eta_1\}\end{aligned} \tag{17}$$

where η_1 is the angle between the line segment OE and the X-axis. The centre coordinate (x_E, y_E) of arc HI can be readily estimated once the values of ξ_0 and δ have been obtained from Eq. (17). Since arc HI is a tangent to the straight line GH at point H, the coordinate of point H can be computed by:

$$\mathbf{r}_H = \{x_E + r_1 \cos\eta_2, y_E + r_1 \sin\eta_2\} \tag{18}$$

where η_2 is the angle between the line segment EH and the X-axis. Once the values of ξ_0 and η_2 have been obtained, the coordinates (x_H, y_H) of point H can be estimated. The shape of arc IJ affects the strength of the cutter teeth and chip removal significantly. Assume that JK is the rear face, KL is the cutting edge strip and the radius of IJ is r_2. The position of point L is associated with the number of helical grooves N in such a way that the circular angle of arc AF becomes $360°/N$. If the cutter has three different helical grooves, point L is $(-R_2 \sin(\pi/6), R_2 \cos(\pi/6)$. If the length of the cutting edge strip KL is n and the clearance angle of the cutting strip is β_e, the equation of line KL can be described as

$$\mathbf{r}_{KL} = \left\{-R_2 \sin\frac{\pi}{6}, R_2 \cos\frac{\pi}{6}\right\} + \xi_1 \left\{\cos\left(\frac{\pi}{6} - \beta_e\right), -\sin\beta_e\right\} \tag{19}$$

where ξ_1 is the length parameter for describing an arbitrary point on segment KL. Let the length of KL be n. The coordinates of point K become

$$\begin{aligned}r_K = \{x_K,y_K\} = \Bigg(&-R_2 \sin\frac{\pi}{6} + n\cos\left(\frac{\pi}{6} - \beta_e\right), \\ &R_2 \cos\frac{\pi}{6} + n \sin\left(\frac{\pi}{6} - \beta_e\right)\Bigg)\end{aligned} \tag{20}$$

If the angle of the straight line JK with the X-axis is given as β_E, then the equation of the straight line DE is

$$\begin{aligned}&\mathbf{r}_{JK} \\ &= \left\{-R_2 \sin\frac{\pi}{6} + n\cos\left(\frac{\pi}{6} - \beta_e\right),\right. \\ &\left. R_2 \cos\frac{\pi}{6} + n\sin\left(\frac{\pi}{6} - \beta_e\right)\right\} \\ &+ \xi_2\{\cos\beta_E, -\sin\beta_E\}\end{aligned} \tag{21}$$

As shown in Fig. 2, line JK is tangent to arc IJ at point J, and arc IJ is tangent to arc HI at point I. If the centre of arc IJ is point F and the radius is r_2, then the coordinates of point F can be given as

$$\begin{aligned}&\mathbf{r}_F = \{x_F,y_F\} = \{x_E + (r_1 + r_2)\cos\nu_3, y_E + (r_1 + r_2)\sin\eta_3\} \\ &= \left\{-R_2 \sin\frac{\pi}{6} + n\cos\left(\frac{\pi}{6} - \beta_e\right) - r_2 \sin\beta_E, R_2 \cos\frac{\pi}{6}\right. \\ &\left. + n\sin\left(\frac{\pi}{6} - \beta_e\right) - r_2 \cos\beta_E\right\} + \xi_2\{\cos\beta_E, -\sin\beta_E\}\end{aligned} \tag{22}$$

where the distance between points E and F is given by $r_1 + r_2$, ϵ_3 is the angle between the line segment EF and the X-axis. Once the values of ξ_2 and η_3 have been obtained from Eq. (22), the coordinates (x_Q, y_Q) of point F can be computed using Eq. (22). The Eq. of arc IJ may be expressed as

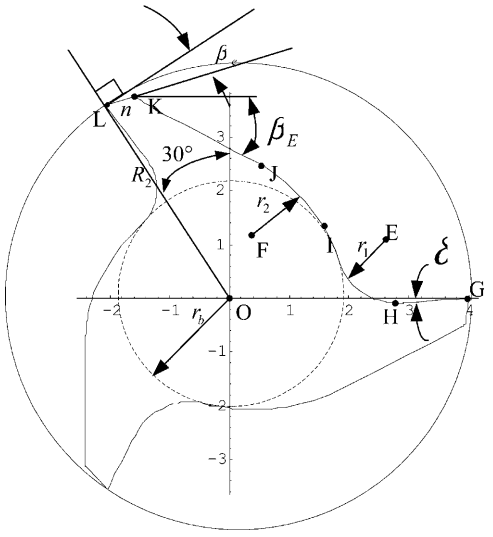

Fig. 2. Section shape of the groove.

$$\mathbf{r}_{IJ} = \{x_F + r_2 \cos\eta_4,\ y_F + r_2 \sin\eta_4\} \tag{23}$$

where η_4 is the angle between line *FI* and line *FM*, and *M* is an arbitrary point on arc *IJ*. Since point *I* is the tangent point of arcs *HI* and *IJ*, the coordinates of point *I* can be obtained readily by solving Eqs (18) and (23) simultaneously. Once the values of η_4 and η_2 have been obtained from the above equation, the coordinates of point *I* can be simply derived. Since line *JK* is tangent to arc *IJ* at point *J*, the coordinates of point J can be computed by solving:

$$\begin{cases} \mathbf{r}_{IJ} = \{x_F + r_2 \sin\eta_4,\ y_F + r_2 \cos\eta_4] \\ \mathbf{r}_{JK} = \left\{-R_2 \sin\dfrac{\pi}{6} + n\cos\left(\dfrac{\pi}{6} - \beta_e\right),\ R_2 \cos\dfrac{\pi}{6} + n\sin\left(\dfrac{\pi}{6} - \beta_e\right)\right\} \\ \quad + \xi_2\{\cos\beta_E,\ -\sin\beta_E\} \end{cases} \tag{24}$$

where the values of η_4 and ξ_2 can be obtained from the previous equations.

According to Eqs (1), (2), and (3), the radius of the revolving surface is variable, i.e. the shape of the grinding wheel is different at different positions. During NC machining of the helical groove, the grinding wheel cannot be changed frequently. The groove should satisfy the function of chip blending and removal, and provide a suitable rake angle and sufficient strength. An accurate shape of the groove is not necessary. Therefore, the groove shape of a cylindrical cutter with a radius of R_2 may define the section of the grinding wheel.

As mentioned above, when the number of grooves is 3, and the cylinder radius is R_2, the equation of the groove section is a sectional continuous function consisting of 5 segments, i.e.

$$\mathbf{r} = \{x(t), y(t)\} = \tag{25}$$

$$\begin{aligned} &\{R_2 - \xi_0 \cos\delta,\ -\xi_0 \sin\delta\} && \text{for } GH \\ &\{x_E + r_1 \cos\nu_2, y_E + r_1 \sin\nu_2\} && \text{for } HI \\ &\{x_F + r_2 \cos\nu_3, y_F + r_2 \sin\nu_3\} && \text{for } IJ \\ &\{x_K + \xi_2 \cos\beta_E, y_K - \xi_2 \sin\beta_E\} && \text{for } JK \\ &\left\{-R_2 \sin\frac{\pi}{6} + \xi_1 \cos\left(\frac{\pi}{6} - \beta_e\right),\ R_2 \cos\frac{\pi}{6} - \xi_1 \sin\beta_e\right\} && \text{for } KL \end{aligned}$$

Let the above flute move along the helix on the cylinder surface. The equation of the helical groove on cylindrical shank may be obtained as follows:

$$\begin{aligned} \mathbf{r}^* &= \{x^*, y^*, z^*\} \\ &= \{x(t)\cos\bar{\theta} - y(t)\sin\bar{\theta}, x(t)\sin\bar{\theta} \\ &\quad + y(t)\cos\bar{\theta}, R_2\bar{\theta}\cot\psi\} \end{aligned} \tag{26}$$

where $\bar{\theta}$ is the revolving angle parameter.

Under the condition of an equidistance transformation angle, it is possible to project the cylinder surface onto a plane such that the normal and the axial profiles may be obtained. Lines *GL* and *OG*, respectively, in Fig. 3 represent these sections. It is important that the radius of the curved line which is followed when performing equidistance transformation is constant, so that the same angle is also conformally mapped and reserved. Therefore, the length of line *GL* is given by the length of the corresponding arc *GL* which is sectioned by the normal groove, and for the case of three grooves, then:

$$GL = \frac{2\pi R_2}{3}\cos\psi \tag{27}$$

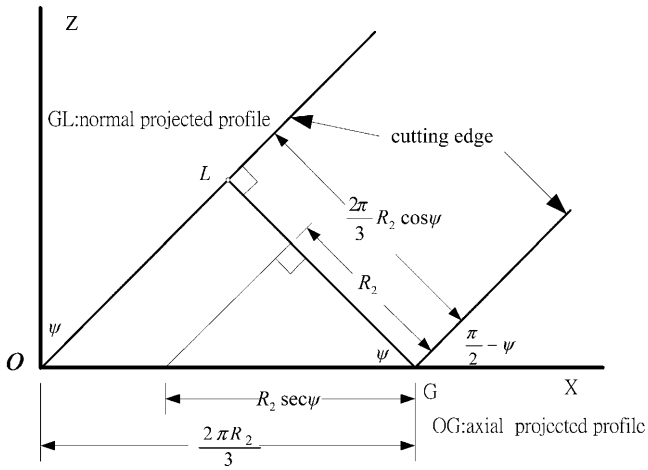

Fig. 3. Relationship between the axial and normal cutting surface.

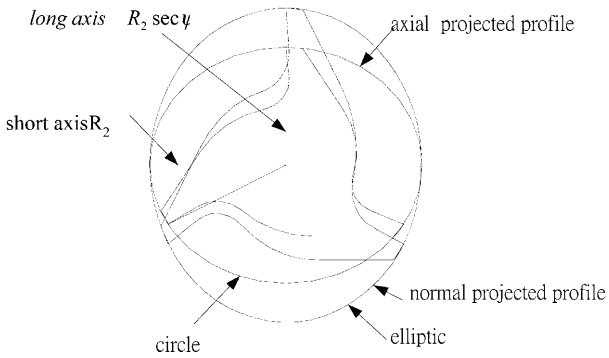

Fig. 4. The axial profile and the cylinder surface form an ellipse with long axis R_2 sec ψ, and short axis R_2.

Therefore, as shown in Fig. 4, the circle on the tangential plane becomes an elliptic shape. In this elliptic shape, the length of the short axis is given as R_2 and the length of the long axis becomes R_2 secψ. The mathematical expression for this elliptic shape can then be given as

$$\eta = \{R_2 \sec\psi \cos\varphi,\ R_2 \sin\varphi\} \tag{28}$$

As given in Fig. 5, the relation of point *L* (R_2 secψ cosφ, R_2 sinφ) on the elliptic curve and length of arc *GL* can be expressed as

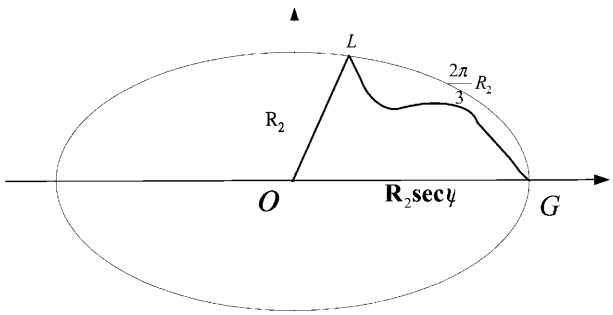

Fig. 5. Ellipse formed by axial profile and cylinder surface.

$$\frac{2\pi}{3} R_2 \cos\psi$$

$$= \int_0^{\varphi} |\epsilon'| d\varphi = \int_0^{\varphi} \sqrt{(R^2{}_2 \sec^2\psi \sin^2\varphi + R^2{}_2 \cos^2\varphi)}\, d\varphi$$

$$= R_2 \int_0^{\varphi} \sqrt{(1 + \tan^2\psi \sin^2\varphi)}\, d\varphi \tag{29}$$

The angular parameter φ at point L can be obtained by integrating the above equations to its upper limit. Thus, the angle LOG can be obtained as

$$\angle LOG = \tan^{-1} \frac{R_2 \sin\varphi}{R_2 \sec\psi \cos\varphi} = \tan^{-1} (\cos\psi \tan\varphi) \tag{30}$$

The design of the corresponding lines *GH*, *HI*, *IJ*, *JK*, and *KL* may be found in the design of the axial profile and are, therefore, not shown here.

5. Sectional Profile Design of the Grinding Wheel

Based upon the design of the groove section, a coordinate system $\sigma_1 = [o_1;x_1,y_1,z_1]$ is constructed, which is associated with the grinding wheel. (see Fig. 6). Let the x_1-axis lie on the x,o,y-plane with an angle of $\pi/6$ to the x-axis. The rake angle δ and the arc BC determine point o_1. Let the axis o_1z_1 of the grinding wheel form an angle $\pi/2-\psi$ with the axis oz of the cutter. o_1z_1 and oz are straight lines which lie on different planes. oo_1 is the common normal vector of o_1z_1 and oz. The equation of o_1z_1 in coordinate system $\sigma = [o;x,y,z]$ can be expressed as:

$$\mathbf{r}_{z_1} = \left\{ \frac{\sqrt{3}}{2} a,\ \tfrac{1}{2}a, 0 \right\} + \mu \left\{ \tfrac{1}{2}\cos\psi, -\frac{\sqrt{3}}{2}\cos\psi,\ \sin\psi \right\} \tag{31}$$

where $a = oo_1$, and is larger than R_2. Since the profile of the grinding wheel is a revolving surface, the normal vector of any point on the revolving surface passes through the axis of rotation. According to the principle of reverse engineering of the envelope, the common normal vector of any point on the instantaneous contact curve between the profile surface of the grinding wheel and the groove surface must pass through the axis of rotation, z_1, i.e.

$$\begin{aligned} \mathbf{r}_{\phi} &= \mathbf{r}^* + \lambda \mathbf{r}_t^* \times \mathbf{r}_{\theta_1}^* \\ &= \{x^* + \lambda N_x,\ y^* + \lambda N_y,\ z^* + \lambda N_z\} \\ &= \mathbf{r}_{z_1} \end{aligned} \tag{32}$$

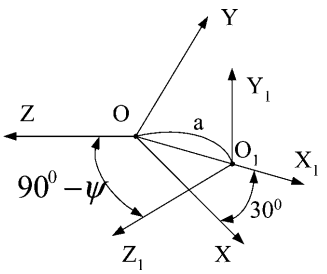

Fig. 6. The relative position between coordinate systems σ and σ_1.

The three components should be equated, respectively, to obtain:

$$\frac{\sqrt{3}}{2} a + \frac{\mu}{2} \cos\psi = x^* + \lambda N_x \tag{33}$$

$$\frac{a}{2} - \frac{\sqrt{3}}{2} \mu \cos\psi = y^* + \lambda N_y \tag{34}$$

$$\mu \sin\psi = z^* + \lambda N_z \tag{35}$$

From Eq. (35), it is known that:

$$\mu = z^* \operatorname{cosec}\psi + \lambda N_z \operatorname{cosec}\psi \tag{36}$$

Substitute μ into Eq. (34), and λ_3 can be obtained:

$$\lambda = \frac{a - \sqrt{3}z \cot\psi - 2y^*}{2N_y + \sqrt{3}N_z \cot\psi} \tag{37}$$

Substitute μ and λ into Eq. (34) to obtain

$$\begin{aligned} &z^* \cot\psi(N_y + \sqrt{3}N_x) \\ &- N_z \cot\psi(\sqrt{3}x^* + y^*) + \\ &a(2N_x \cot\psi + \sqrt{3}N_y - N_x) \\ &+ 2(y^*N_x - x^*N_y) = 0 \end{aligned} \tag{38}$$

By using the following property of a spiral surface:

$$y^*N_x - x^*N_y = bN_z \tag{39}$$

where b is the spiral parameter, and $b = R_2 \cot\psi$ is the situation where a point on the groove surface is also on the profile of the grinding wheel can be expressed as:

$$\begin{aligned} &z^* \cot\psi(N_y + \sqrt{3}N_x) \\ &- N_z \cot\psi(\sqrt{3}x^* + y^*) \\ &+ a(2N_x \cot\psi + \sqrt{3}N_y - N_x) + 2bN_z \\ &= 0 \end{aligned} \tag{40}$$

From Eq. (40), the contact curve between the profile of the grinding wheel and the spiral groove may be given as:

$$\mathbf{r}_{\theta} = \{x(\bar{\theta}), y(\bar{\theta}), z(\bar{\theta})\} \tag{41}$$

In order to express the contact curve of Eq. (41) of the coordinate system $\sigma_1 = [o;x_1,y_1,z_1]$ in terms of $\sigma' = [o;x',y',z']$, we will have to rotate the coordinate system $\sigma = [o;x,y,z]$ around the z-axis through an angle of $\pi/6$. The transformation from $\sigma = [o;x,y,z]$ to $\sigma' = [o;x',y',z']$ is as follows:

$$\begin{aligned} x' &= \tfrac{1}{2}\, x(\bar{\theta}) + \frac{\sqrt{3}}{2}\, y(\bar{\theta}) \\ y' &= -\frac{\sqrt{3}}{2}\, x(\bar{\theta}) + \tfrac{1}{2}\, y(\bar{\theta}) \\ z' &= z(\bar{\theta}) \end{aligned} \tag{42}$$

The transmission from $\sigma' = [o;x',y',z']$ to $\sigma_1 = [o;x_1,y_1,z_1]$ is given as:

$$\begin{aligned} x_1 &= x' - a \\ y_1 &= y' \sin\psi + z' \cos\psi \\ z_1 &= y' \cos\psi + z' \sin\psi \end{aligned} \tag{43}$$

Therefore, the contact curve can be expressed in the coordinate system $\sigma_1 = [o;x_1,y_1,z_1]$ as

$$x_1 = \tfrac{1}{2}\, x(\bar{\theta}) + \frac{13}{2}\, y(\bar{\theta}) - a$$
$$y_1 = -\frac{\sqrt{3}}{2}\, x(\bar{\theta})\, \sin\psi + \tfrac{1}{2}\, y(\bar{\theta})\, \sin\psi + z(\bar{\theta})\, \cos\psi \tag{44}$$
$$z_1 = \frac{\sqrt{3}}{2}\, x(\bar{\theta})\, \cos\psi - \tfrac{1}{2}\, y(\bar{\theta})\, \cos\psi + z(\bar{\theta})\, \sin\psi$$

By rotating the contact curve of Eq. (44) around the z_1-axis, the connection of intersecting point between the profile surface and the plane $y_1 = 0$ immediately leads to the profile curve of the grinding wheel. The profile curve can thus be expressed as

$$\mathbf{r}_c = \{x_c, 0, z_c\} = \{(x_1^2 + y_1^2)^{1/2}, 0, z_1\} \tag{45}$$

6. Feed Speed of the Grinding Wheel in NC Machining

Let the angular speed ω of the cutter be constant, i.e.

$$\omega = \mathrm{d}\phi/\mathrm{d}t = \text{Constant} \tag{46}$$

The speed v_z in the axial direction can be calculated by:

$$v_z = \frac{\mathrm{d}z}{\mathrm{d}t} \tag{47}$$

For the revolving surface formed by arc AB, we obtain:

$$v_{z1} = \frac{\mathrm{d}z_1}{\mathrm{d}t} = \omega\, \frac{R^2 - z^2}{R}\, \cot\psi \tag{48}$$

If the radial feed speed of the grinding wheel varies linearly with the variation of radius, overcut will occur. Since the grinding wheel is designed based upon the maximum radius of the cylinder, the displacement in the direction of the radial feed should be modified as follows:

$$S_g = r_b - \frac{r_b}{R_2}\, \sqrt{(x^2 + y^2)} \tag{49}$$

By using Eq. (8), it will be found that the radial speed of the grinding wheel is as follows:

$$v_{g_1} = \frac{\mathrm{d}S_{g_1}}{\mathrm{d}t} = -\frac{r_b}{R_2}\, \frac{\mathrm{d}\sqrt{(R^2 - z^2)}}{\mathrm{d}t} = \frac{1}{RR_2}\, r_b\, z\omega\, \cot\psi\, \sqrt{(R^2 - \mathrm{z}^2)} \tag{50}$$

For the revolving surface formed by the arc BC, we obtain:

$$v_{z_2} = \frac{\mathrm{d}z_2}{\mathrm{d}t} = \omega\, \cot\psi\, \cos\theta_1\, (R + R_1 - R_1\, \cos\theta) \tag{51}$$

The displacement in the direction of radial feed should be modified as follows:

$$S_{g_2} = r_b - \frac{r_b}{R_2}\, (R + R_1 - R_1\, cos\theta) \tag{52}$$

The radial feed speed is given by the following:

$$v_{g_2} = -\frac{1}{R_2}\, r_b\, \omega\, \cot\psi\, \sin\theta_1\, (R + R_1 - R_1\, \cos\theta) \tag{53}$$

At the conjunction of the two cutting edges, $\theta = \pi/2, \theta_1 = 0$ and we obtain:

$$v_{z_1} = \omega R\, \cot\psi = v_{z_2} \tag{54}$$
$$v_{g_1} = 0 = v_{g_2} \tag{55}$$

7. The Groove Surface

The equations of the grinding wheel profile is:

$$\hat{\mathbf{r}} = \{x_c\, \cos\nu,\, x_c\, \sin\nu,\, z_c\} = \{\hat{x}, \hat{y}, \hat{z}\} \tag{56}$$

Expressed in the coordinate system σ, Eq. (56) becomes Eq. (57), i.e.

$$\begin{cases} x = \tfrac{1}{2}\, (x_c\, \cos\nu + a) - \dfrac{\sqrt{3}}{2}\, (x_c\, \sin\nu\, \sin\psi - z_c\, \cos\psi) \\ y = \dfrac{\sqrt{3}}{2}\, (x_c\, \cos\nu + a) + \tfrac{1}{2}\, (x_c\, \sin\nu\, \sin\psi - z_c\, \cos\psi) \\ z = x_c\, \sin\nu\, \cos\psi + z_c\, \sin\psi \end{cases} \tag{57}$$

Considering the combined effects of ω, V^*_g and V_z, the equation of the grinding wheel profile is:

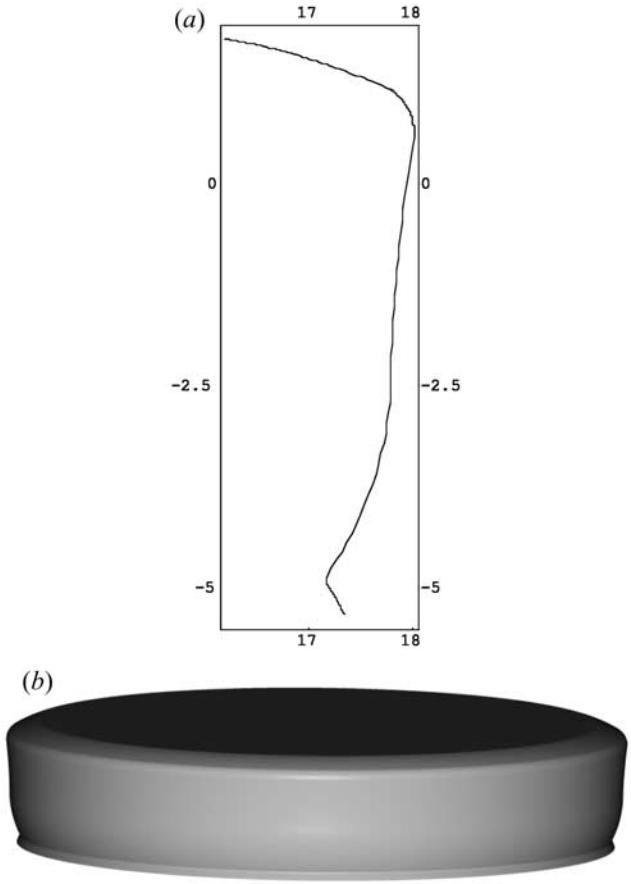

Fig. 7. (*a*) The sectional profile of the grinding wheel. (*b*) The grinding wheel.

$$\begin{cases} x^{**} = \left(x + \frac{1}{2}\int_0^z V_g^* \, dz\right)\cos\phi - \left(y + \dfrac{\sqrt{3}}{2}\int_0^z V_g^* \, dz\right)\sin\phi \\ y^{**} = \left(x + \frac{1}{2}\int_0^z V_g^* \, dz\right)\sin\phi + \left(y + \dfrac{\sqrt{3}}{2}\int_0^z V_g^* \, dz\right)\cos\phi \\ z^{**} = \left(z + \frac{1}{2}\int_0^z V_z \, dz\right) \end{cases} \quad (58)$$

where ϕ is defined by Eq. (9). With the effect of enveloping, the actual surface of the groove at the ball-end part is defined by Eq. (59), i.e.

$$\begin{cases} \mathrm{r}^{**} = \{x^{**}, y^{**}, z^{**}\} \\ (\mathbf{r}_{x_c}^{**}, \mathbf{r}_v^{**}, \mathbf{r}_{z_c}^{**}) = 0 \end{cases} \quad (59)$$

This may also be expressed as:

$$\begin{vmatrix} x_{x_c}^{**} & y_{x_c}^{**} & z_{x_c}^{**} \\ x_v^{**} & y_v^{**} & z_v^{**} \\ x_{z_c}^{**} & y_{z_c}^{**} & z_{z_c}^{**} \end{vmatrix} = 0 \quad (60)$$

Since the full derivation of $(\mathbf{r}_{x_c}^{**}, \mathbf{r}_v^{**}, \mathbf{r}_{z_c}^{**})$ is rather lengthy, only the final expression is given here, i.e.

$$(\mathbf{r}_{xc}^*, \mathbf{r}_v^*, \mathbf{r}_z^*) = 0 \text{ or } (\mathbf{r}_{xc}^*, \mathbf{r}_v^*, \mathbf{r}_{\theta_1}^*) = 0 \quad (61)$$

From Eq. (61), the feed speeds of the grinding wheel are continuous. We know that the detailed expressions of Eqs (60) and (61) are very complicated. In fact, x_c is discrete, and the surface of the groove actually obtained can be defined by numerical methods. Since the full derivation of $(\mathbf{r}_{x_c}^{**}, \mathbf{r}_v^{**}, \mathbf{r}_{z_c}^{**}) = 0$ is rather lengthy, only the final expression is given here, i.e.

$$\begin{aligned} \mathbf{r}^{**} = \{ & x_c \cos v \cos\left(\frac{\pi}{6} + \phi\right) - x_c \sin v \\ & \sin\psi \sin\left(\frac{\pi}{6} + \phi\right) + a \cos\left(\frac{\pi}{6} + \phi\right) \\ & + z_c \cos\psi \sin\left(\frac{\pi}{6} + \phi\right) + \left(r_b - \frac{r_b}{R_2} f(u)\right) \\ & \cos\left(\frac{\pi}{6} + \phi\right) x_c \cos v \sin\left(\frac{\pi}{6} + \phi\right) \\ & + x_c \sin v \sin\psi \cos\left(\frac{\pi}{6} + \phi\right) + a \sin\left(\frac{\pi}{6} + \phi\right) \\ & - z_c \cos\psi \cos\left(\frac{\pi}{6} + \phi\right) + \left(r_b - \frac{r_b}{R_2} f(u)\right) \\ & \sin\left(\frac{\pi}{6} + \phi\right) x_c \sin v \cos\psi + z_c \sin\psi + g(u)\} \end{aligned} \quad (62)$$

$$\begin{aligned} & a \cos\psi + \left(r_b - \frac{r_b}{R_2} f(u)\right)\cos\psi + a z'_c \sin v \sin\psi \\ & + z_c z'_c \cos v \cos\psi \end{aligned} \quad (63)$$

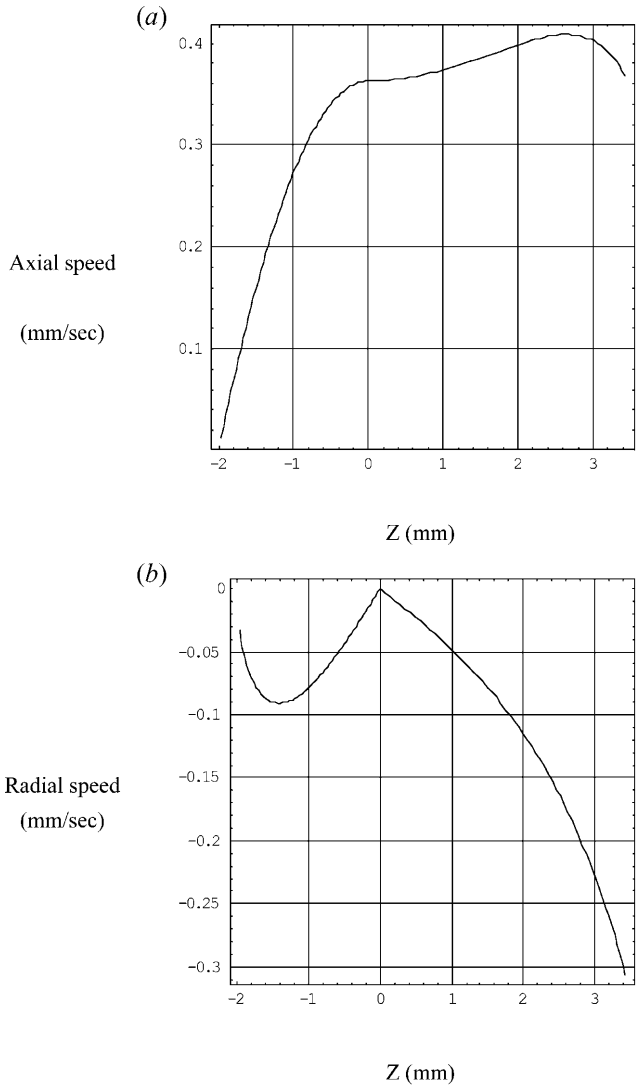

Fig. 8. Feed speed of the grinder in (*a*) the axial and (*b*) the radial directions.

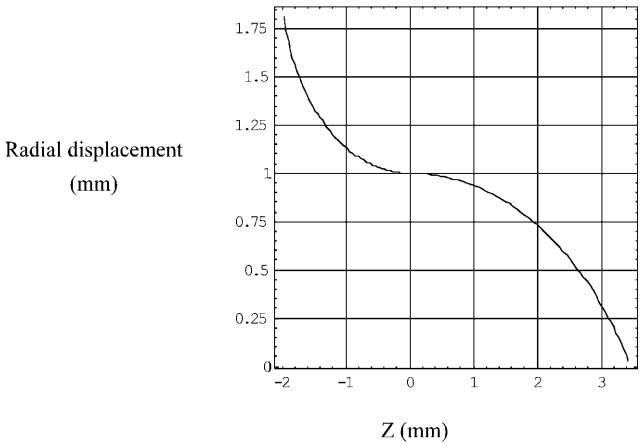

Fig. 9. The radial displacement of the grinding wheel.

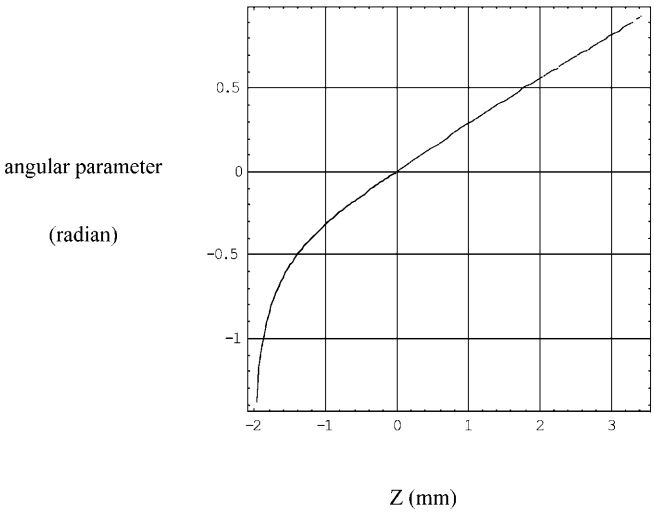

Fig. 10. The angular parameter of revolving surface.

$$+ z'_c \left(r_b - \frac{r_b}{R_2} f(u) \right) \sin v \sin\psi + x_c$$

$$\cos v \cos\psi + \left(v_g z'_c \cos v + \right.$$

$$\left. v_z z'_c \sin v \cos\psi - v_z \sin\psi \right) \frac{du}{d\phi} = 0$$

where

$$z'_c = \frac{dz_c}{dx_c} \tag{64}$$

The equation of the sphere is given as:

$$f(u) = \sqrt{(R^2 - z^2)},\ g(u) = z \tag{65}$$

$$\frac{du}{d\phi} = \frac{dz}{d\phi} = \frac{R^2 - z^2}{R} \cot\psi \tag{66}$$

The equation of the concave-arc is given as:

$$f(u) = R + R_1 - R_1 \cos\theta_1\ g(u) = R_1 \sin\theta_1 \tag{67}$$

$$\frac{du}{d\phi} = \frac{d\theta_1}{d\phi} = \frac{R + R_1 - R\cos\theta_1}{R_1} \cot\phi \tag{68}$$

8. Computer Simulation and Remedy

Applying the models given above, the cutting edge and groove surface actually obtained may be simulated by a computer. The key issues include three aspects:

1. The actual and theoretical cutting edge.
2. The section curves of the groove actually obtained at different positions.
3. Whether a not overcut occurs or if a residual revolving surface is present.

In order to simulate the results of the cutting edge, given a series of value of z_i, from Eqs (1) or (5), the section radius can be defined by $r_i = \sqrt{(x_i^2 + y_i^2)}$. From the following equation:

$$\begin{aligned} \sqrt{(x_i^{*2} + y_i^{*2})} &= r_i \\ z^* &= z_i \\ (\mathbf{r}^*_{xc}, \mathbf{r}^*_v, \mathbf{r}^*_u) &= 0 \end{aligned} \tag{69}$$

we can calculate a series of values of (x_c,v,z). These are substituted into Eqs (62) – (68), to obtain a series of points on the cutting edge.

A CABEM milling cutter is selected as one example to illustrate the effectiveness of the proposed mathematical modelling and residual compensation method. The cutter has a helical angle of $\pi/3$, a rake angle of $\delta = 5°$, the radius of groove arc HI of $r_1 = 1$ mm, the radius of groove arc IJ of $r_2 = 2$ mm, the length of the cutting edge strip of $n = 0.5$ mm, the clearance angles of the cutting strip of $\beta_e = 6°$ and $\beta_E = 30°$, the distance between o and o_1 of $a = 20$ mm, cylindrical radius of 4 mm, and the remaining circular end radius of 2 mm. The modelling and residual compensation methods proposed above are used to design and produce the high-precision CABEM cutter systematically on a simple two-axis NC machine. The sectional profile of helical grooves on the cylinder shank of the CABEM cutter is given in Fig. 2. The grinding wheel and sectional profile are Fig. 7. Figure 8 shows the feed speed of the grinder in both the axial and the radial directions. Figure 9 shows the radial displacement of the grinding wheel. Figure 10 shows the angular parameter of the revolving surface.

In order to obtain the shape of the groove at different sections v_i may be obtained from Eq. (63) for different values of x_c. Substituting v_i into Eq. (62), given a series of points on the section.

The actual cutting edge obtained and the cutting edge designed are as shown in Fig. 11. It can be seen that the actual cutting edge is slightly different from the designed cutting edge.

According to the above simulation results, the residual revolving surface may be rectified by the following approach.

A cone-shaped grinding wheel with a bottom angle of $\pi/2 - \beta_e$ is used to eliminate the residual revolving surface. The relative positions of the grinding wheel and the cutter are shown in Fig. 12. While maintaining constant axial and revolving speeds, the radial speed v_g is modified by a factor λ_0, since the actual point (x^*, y^*) on the cutting edge is different from the designed point $(x., y)$. From the relationship between the designed point and the obtained point (as shown in Fig. 13), the following equation exists:

$$\begin{aligned} &\{x,y\}\{\lambda_0 x - x^*, \lambda_0 y - y^*\} \\ &- \sqrt{(x^2 + y^2)}\ \sqrt{((\lambda_0 x - x^*)^2 + (\lambda_0 y - y^*)^2)}\ \sin\beta_e = 0 \end{aligned} \tag{70}$$

From Eq. (70), factor λ_0 may be defined. The revised radial speed may be calculated from:

$$\bar{v}_g = \frac{d(\lambda_0 f)}{dt} = \frac{d(\lambda_0 \sqrt{(x^2 + y^2)})}{dt} \tag{71}$$

By replacing v_g with $\bar{v}_g$, the residual surface can be eliminated. The problem of the narrow cutting edge strip can also be solved. Since the designed point $(x., y)$ is approximate to the actual point (x^*, y^*), the actual relief angle is approximate to the designed value, and so an ideal special revolving cutter is obtained.

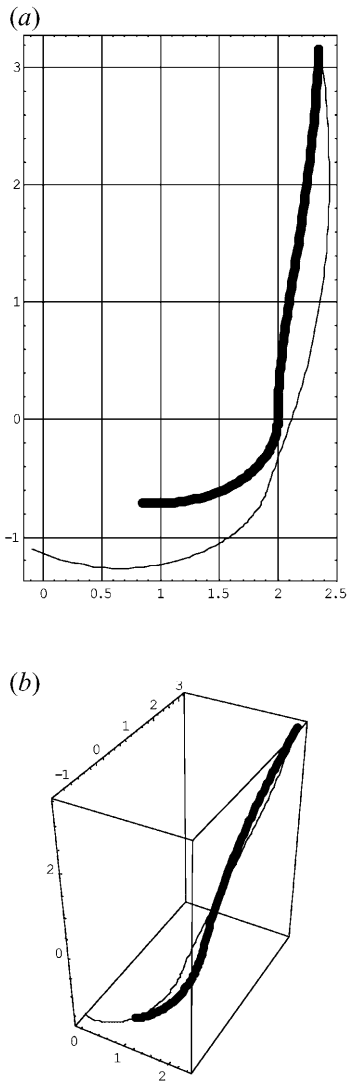

Fig. 11. The actual and desired (thick line) cutting edge curve. (*a*) The projected cutting edge curve of the CABEM on the *X*,*Y*-plane. (*b*) The spatial cutting edge curve of the CABEM.

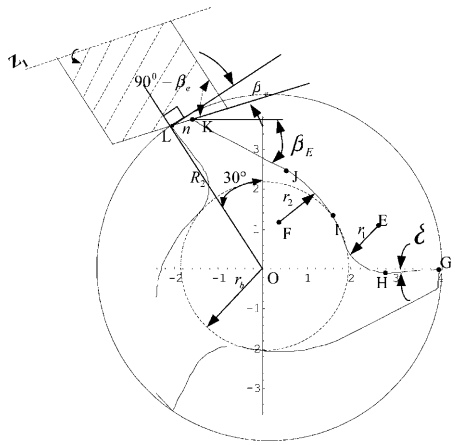

Fig. 12. The relative position between the grinding wheel and the cutter.

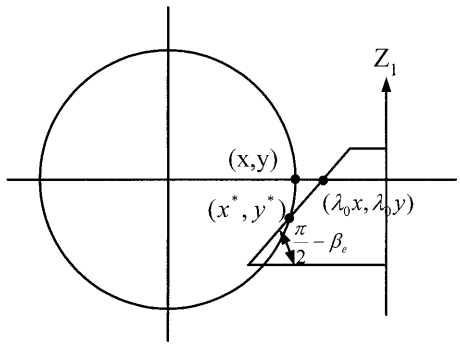

Fig. 13. The definition of the adjusted wheel angle λ_0.

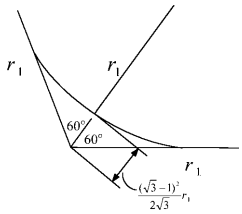

Fig. 14. The geometric model of overcutting by grinding wheel.

Considering the ball-end part, it will be seen that overcut begins when the groove has an angle of $2\pi/3$, and that overcut increases towards the tip of the ball-end. Therefore, it is necessary to change the grinding wheel when machining this area, as shown in Fig. 14, it is known that when:

$$f < \frac{(\sqrt{3}-1)^2}{2\sqrt{3}}\, r_1 \frac{R_2}{r_b} \tag{72}$$

overcut will occur. If:

$$f = \frac{(\sqrt{3}-1)^2}{2\sqrt{3}}\, r_1 \frac{R_2}{r_b} \tag{73}$$

gives $z = z^*$, then the grinding wheel should be changed to the one shown in Fig. 15, and grinding should continue until the edge profile of the ball-end is complete. The start point (x^*,y^*,z^*) is obtained by substituting $z = z^*$ into Eqs (62) and (63).

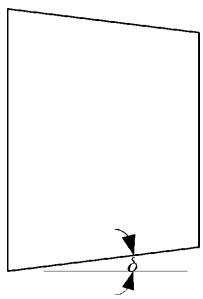

Fig. 15. The cone-shaped grinding wheel with rake angle δ.

9. Conclusions

From the related models and the simulated results, it is known that the design and manufacture of a ball-end cutter with a concave-arc generator presents many difficulties and requires much conventional skill. If a method is used to machine the rake face and the groove separately, the process is very complicated. This paper provides an effective 2-axis NC machining approach for, so that an ideal ball-end cutter with a concave-arc generator may be obtained through the proper control of the feed speeds of the grinding wheel in the radial and axial direction. This paper presents a low-cost method for the design and NC machining of this type of cutter.

References

1. A. Barsov, Cutting Tool Production, Moscow, Mir, 1978.
2. A. Y. Hidehj, "Development of elliptic ball-end mill", Bulletin Japan Society of Precision Engineers, 20(4), pp. 59–66, 1986.
3. A. V. Kataev, "Computer aided design of tool with complex forming faces", Soviet Engineering, 9(7), pp. 22–28, 1989.
4. S. Kaldor, P. H. H. Trendler and T. Hodgson, "Investigation and optimization of the clearance geometry of end mills", Annals CIRP, 34(1), pp. 153–159, 1985.
5. S. K. Kang, K. F. Ehmann and C. Lin, "A CAD approach to helical groove machining mathematical model and model solution", International Journal of Machine Tools and Manufacture, 36(1), pp. 141–153, 1996.
6. H. S. Yan and J. Y. Lin, "Geometric design and machining of variable pitch lead screws with cylindrical meshing elements", Transactions ASME, Journal of Mechanical Design, 115, pp. 490–495, 1993.
7. P. D. Lin and M. F. Lee, "NC data generation for 4-axis machine tools equipped with rotatory angle head attachments to produce variable pitch screws", International Journal of Machine Tools and Manufacture, 37(3), pp. 341–353, 1997.
8. S. Kaldor, A. M. Rafael and D. Messinger, "On the CAD of profiles for cutters and helical flutes-geometrical aspects," Annals CIRP, 37(1), pp. 53–57, 1988.
9. D. S. Sheth and S. Malkin, "CAD/CAM for geometry and process analysis of helical groove machining", Annals CIRP, 39(1), pp. 129–132, 1991.
10. M. Y. Friedman and M. Meister, "The profile of a helical slot machined by a form-milling cutter", Annals CIRP, 22(1), pp. 157–164, 1973.
11. M. Y. Yang and H. D. Park, "The prediction of cutting force in ball-end milling", International Journal of Machine Tools and Manufacture, 31(1), pp. 45–54, 1991.
12. G. Yucesan and Y. Altintas, " Prediction of ball-end milling forces", Journal of Engineering for Industry, 118(2), pp. 95–103, 1996.
13. C. C. Tai and K. H. Fuh, "Model for cutting forces prediction in ball-end milling", International Journal of Machine Tools and Manufacture, 35(4), pp. 511–524, 1995.
14. P. Lee and Y. Altintas, "Prediction of ball-end milling forces from orthogonal cutting data", International Journal of Machine Tools and Manufacture, 36(9), pp. 1059–1063, 1996.
15. Y. Gardon, Mathematics and CAD: Numerical Methods for CAD, MIT Press, Cambridge, Massachusetts, 1986.
16. H. R. Liu, "The smooth conjunction of cutting edge ball-end milling cutter", Tool Engineering, 29(2), pp. 11–13, 1995.
17. C. X. Zhou, Q. Shen and M. Wang, "Mathematical models for NC machining of special revolving cutter – the forming methods of the planar rake plane", Journal of Southeast University, 25(2), pp. 25–29, 1995.
18. C. X. Zhou, D. Q. Yue and X. T. Wu, "The forming principle of special revolving cutter with planar rake plane", Tool Engineering, 25(5), pp. 17–21, 1991.
19. L. F. Li, "Calculating the normal section of helical groove of the cutter by computer", Tool Engineering, 9, pp. 15–19, 1995.
20. D. Q. Yue, "The new process of manufacturing the helical groove of taper cutter", Tool Engineering, 1, pp. 1–10, 1984.
21. D. C. Kang, X. Xv and N. X. Yao, "Calculating and measurement of cutting parameters of gear mill with helical groove", Tool Engineering, 5, pp. 15–20, 1994.
22. J. Y. Liu, "Study on geometric modeling and theory about NC machining of special revolving tool", Dissertation of Harbin Institute of Technology, August 1998.
23. Y. Y. Tang and C. K. Chen, "Geometry model and 2-axis NC machining of milling cutters with constant helical angle", Journal of Harbin Institute of Technology, 28(5), pp. 5–7, 1996.
24. H. Zhang and N. X. Yao, "The general algorithm of cutting edge of revolving cutter with constant helical angle", Journal of Dalian Institute of Technology, 31(1), 1997. pp. 63–67, 1997.
25. Y. X. Li and Y. W. Dong, "The optimization design of section of ball-end cutter – orthogonal testing", Tooling Engineering, 11, pp. 36–38, 1987.
26. J. Y. Liu and H. M. Liu, "Mathematical model of helical flutes of cone milling cutter", Tooling Engineering, 4, pp. 3–6, 1997.

Nomenclature

a	distance between o and o_1 (origin of $\boldsymbol{\sigma}$ and $\boldsymbol{\sigma}_1$)
b	parameter of helix
C	integration constant
E	coefficients of first fundamental form ($= \mathbf{r}_z^2$)
F	coefficients of first fundamental form ($= \mathbf{r}_z \bullet \mathbf{r}_\phi$)
G	coefficients of first fundamental form ($=\mathbf{r}_\phi^2$)
N	number of helical grooves
N_x,N_y,N_z	components of normal cross of $\mathbf{r}_t$ and $\mathbf{r}_\theta$
n	length of cutting edge strip KL
R	radius of sphere surface
R_1	radius of generator of concave-arc
R_2	maximum revolving radius of cutter
$\mathbf{r}_1$	equation of revolving surface corresponding to arc AB
$\mathbf{r}_2$	equation of revolving surface corresponding to arc BC
$\mathbf{r}_3$	equation of revolving surface corresponding to line CD
r_1	radius of arc HI of groove
r_2	radius of arc IJ of groove
r_b	radius of inner land circle
$\mathbf{r}_c$	sectional profile of grinding wheel
$\mathbf{r}_\phi$	profile equation of grinding wheel in wheel coordinate system σ_1
$\mathbf{r}_{z_1}$	equation of line o_1z_1 in terms of coordinate system σ
$\mathbf{r}^*$	equation of helical groove of cylinder part
$\bar{\mathbf{r}}_\theta$	contact curve between the profile of the grinding wheel and the spiral groove
$\mathbf{r}^{**}$	actual surface of groove
$\mathrm{d}\mathbf{r}$	tangent vector of cutting edge
S	radial displacement of grinding wheel
V_g	radial feed speed of grinding wheel
V_z	axial feed speed of grinding wheel
$\hat{V}_g$	modified radial feed speed of grinding wheel
$\overline{V}_g$	radial feed speed of the grinding wheel with a bottom angle of $90° - \beta_e$
$\{x,y,z\}$	equation of revolving surface of cutter

$\{x_1,y_1,z_1\}$	contact curve of wheel coordinate system
$\{x_c,0,z_c\}$	sectional profile of grinding wheel
$\{x_\phi,y_\phi,z_\phi\}$	profile equation of grinding wheel in wheel coordinate system
$\{x^*,y^*,z^*\}$	equation of helical groove of cylinder part
$\{x^{**},y^{**},z^{**}\}$	actual surface of groove
$\{x(\bar{\theta}),y(\bar{\theta}),z(\bar{\theta})\}$	contact curve between profile of grinding wheel and spiral groove
β_e	clearance angle of cutting strip
β_E	angle of straight line *JK* to *X*-axis
δ	rake angle
ψ	helical angle between tangent vector of helical curve and tangent vector of longitude curve
ϕ	angular parameter of revolving surface
ϕ_0	initial angle of ϕ
$\eta_1,\eta_2,$ η_3,η_4	anglar parameter of circular arc
λ_0	actual modified radial feed speed parameter of grinding wheel
λ	length parameter
μ	length parameter
θ_1	angular parameter of toroid revolving surface
θ_2	angular parameter of revolving surface formed by concave-arc
σ	coordinate system attached to pinion cutter
σ_1	coordinate system attached to grinding wheel
σ^1	temporary coordinate system; σ rotates 30° around *z*-axis
ω	revolving angular velocity of cutter
ξ_0,ξ_1,ξ_2	length parameter